How Do Volcanic Eruptions Influence Decadal Megadroughts over Eastern China?

LIANG NING,[a,b,c,d] KEFAN CHEN,[a] JIAN LIU,[a,b,e] ZHENGYU LIU,[f] MI YAN,[a,b,d] WEIYI SUN,[a] CHUNHAN JIN,[a] AND ZHENGGUO SHI[d]

[a] *Key Laboratory for Virtual Geographic Environment, Ministry of Education, and State Key Laboratory Cultivation Base of Geographical Environment Evolution of Jiangsu Province, and Jiangsu Center for Collaborative Innovation in Geographical Information Resource Development and Application, and School of Geography, Nanjing Normal University, Nanjing, China*
[b] *Open Studio for the Simulation of Ocean-Climate-Isotope, Qingdao National Laboratory for Marine Science and Technology, Qingdao, China*
[c] *Climate System Research Center, Department of Geosciences, University of Massachusetts, Amherst, Massachusetts*
[d] *State Key Laboratory of Loess and Quaternary Geology, Institute of Earth Environment, Chinese Academy of Sciences, Beijing, China*
[e] *Jiangsu Provincial Key Laboratory for Numerical Simulation of Large Scale Complex Systems, School of Mathematical Science, Nanjing Normal University, Nanjing, China*
[f] *Department of Geography, The Ohio State University, Columbus, Ohio*

(Manuscript received 31 May 2019, in final form 6 July 2020)

ABSTRACT

The influence and mechanism of volcanic eruptions on decadal megadroughts over eastern China during the last millennium were investigated using a control (CTRL) and five volcanic eruption sensitivity experiments (VOLC) from the Community Earth System Model (CESM) Last Millennium Ensemble (LME) archive. The decadal megadroughts associated with the failures of the East Asian summer monsoon (EASM) are associated with a meridional tripole of sea surface temperature anomalies (SSTAs) in the western Pacific from the equator to high latitudes, suggestive of a decadal-scale internal mode of variability that emerges from empirical orthogonal function (EOF) analysis. Composite analyses further showed that, on interannual time scales, within a decade after an eruption the megadrought was first enhanced but then weakened, due to the change from an El Niño state to a La Niña state. The impacts of volcanic eruptions on the magnitudes of megadroughts are superposed on internal variability. Therefore, the evolution of decadal megadroughts coinciding with strong volcanic eruptions demonstrate that the impacts of internal variability and external forcing can combine to influence hydroclimate.

1. Introduction

Megadroughts have profound impacts on agriculture, water resources, ecosystems, and the societal development due to their long persistence and severe magnitudes (Zheng et al. 2006; Cook et al. 2016; Yang et al. 2017a). Much of our knowledge of megadroughts in the last millennium comes from tree-ring-based reconstructions of summer wetness and dryness, including the North American Drought Atlas (NADA) (Cook et al. 2004), Monsoon Asia Drought Atlas (MADA) (Cook et al. 2010), Old World Drought Atlas (OWDA) (E. R. Cook et al. 2015), Mexican Drought Atlas (Stahle et al. 2016), and Australia–New Zealand Drought Atlas (ANZDA) (Palmer et al. 2015).

Due to increasing temperature, the occurrence risk of megadroughts and other extreme events over some regions is predicted to increase (Ning and Bradley 2015; Ault et al. 2016; Stevenson et al. 2018). For example, based on an empirical drought reconstruction and general circulation models, B. I. Cook et al. (2015) indicated that the American Southwest and Central Plains are expected to experience increased drought severity in the coming decades in response to future warming. Ault et al. (2014, 2016) also draw similar conclusions from model simulations

Denotes content that is immediately available upon publication as open access.

Supplemental information related to this paper is available at the Journals Online website: https://doi.org/10.1175/JCLI-D-19-0394.s1.

Corresponding author: Jian Liu, jliu@njnu.edu.cn

DOI: 10.1175/JCLI-D-19-0394.1

and paleoclimate data. They suggest that the risk of megadrought over the United States will increase in the future, bringing severe challenges to regional water resources.

For a more accurate assessment of the likelihood of megadrought occurrence in the future, it is critical to improve our understanding of the mechanisms that trigger and maintain megadroughts. In general, megadroughts can be caused by internal climate variability in the absence of external forcings. This can be seen in the analysis of a 1000-sample linear inverse model based on global sea surface temperature anomalies (SSTAs) and self-calibrated Palmer index data over North America (Ault et al. 2018). In comparison of a fully coupled control run with an atmosphere-only run forced by the SST climatology from the control, Stevenson et al. (2015) also found that many decadal megadroughts over the United States are caused by a combination of internal atmospheric variability and coupling with the land surface. In comparison of transient simulations forced by external forcings and preindustrial control runs, Coats et al. (2015) also suggested that the simulated megadroughts are not forced by changes in the external forcings.

Over eastern China, previous studies based on paleoproxy records (e.g., Yancheva et al. 2007; Zhang et al. 2008; D. Zheng et al. 2010) found that megadroughts were associated with the weakening of the East Asian summer monsoon (EASM). This mechanism is consistent with the work of Cook et al. (2010), which further finds that the weakening EASM is closely associated with large-scale patterns of tropical Indo-Pacific SSTAs. Yang et al. (2017a,b) also found that the PDO-like SSTA pattern is important in modulating the decadal variability of a north–south dipole pattern of precipitation anomaly over eastern China, and this influence is achieved through a large-scale cyclonic circulation pattern in the lower troposphere over the entire northern part of the North Pacific. Zhang and Zhou (2015) also found that droughts in the recent decades over northern China result from a weakening tendency of the EASM, which is mainly induced by the PDO phase transition.

On the other hand, external forcings (e.g., volcanic eruptions) can also influence the risk and persistence of megadroughts over eastern China through alterations of large-scale teleconnections (Ning et al. 2018; Stevenson et al. 2018). For example, it has been suggested that three exceptional drought events over eastern China during the last five centuries might be triggered by large volcanic eruptions, and then further amplified by El Niño events (Shen et al. 2007). By comparing proxy data and model simulations, Peng et al. (2014) indicated that solar activity may be the primary driver of the occurrences of several megadroughts during the last millennium over eastern China. Stevenson et al. (2016) found that the Asian monsoon can be suppressed by both volcanic eruptions and El Niño, which induce northeasterly wind anomalies along the southeastern coast of China and suppress convection over the equatorial western Pacific due to a weaker Walker circulation, consistent with the simulations from Man et al. (2014). Ning et al. (2017) also found that continuous volcanic eruptions can cause decadal decreases of Asian summer monsoon precipitation by inducing a negative AMO-like SSTA pattern and a decadal El Niño–like SSTA pattern. Stevenson et al. (2018) also indicate that volcanic influences droughts, in part, by enhancing the AMO amplitude as well as changing the teleconnections associated with both AMO and ENSO.

Previous studies in both proxy reconstructions and model simulations show that strong volcanic eruptions can force significant El Niño events in the tropical Pacific (e.g., Adams et al. 2003; Mann et al. 2005; Stevenson et al. 2016; Lu et al. 2018). A recent study on both proxy data and model simulations further suggests that a significant La Niña state emerges in the second year after strong tropical volcanic eruptions following the El Niño conditions (Sun et al. 2019). Moreover, volcanic eruptions play a key role in not only the phasing and magnitude of AMO (e.g., Otterå et al. 2010; Swingedouw et al. 2015; Stevenson et al. 2018), but also the phasing of PDO, with the North Pacific entering the negative PDO phase after an eruption and persisting for several years (Wang et al. 2012). These previous studies have focused on the response of the coupled atmosphere–ocean system to volcanic eruptions across a range of time scales over the Pacific. However, it has remained little studied how the response in the Pacific further influences megadroughts in eastern China.

In this study, we will focus on how volcanic eruptions impact megadroughts in eastern China, in combination with internal climate variability. We will study the features at both decadal and interannual time scales (i.e., occurrence and evolution) for decadal megadroughts in eastern China in response to strong volcanic eruptions, and the associated mechanisms. In particular, we will focus on the evolution of decadal megadroughts that concur with strong volcanic eruptions. Our results show that the megadrought can be caused by the combined influences of both internal variability and external forcings. The paper is arranged as follows. Section 2 describes the data and methodology. The influences of volcanic eruptions on megadroughts over eastern China and corresponding mechanisms are examined in section 3. Potential reasons for the discrepancies between reconstructions and modeling on monsoon responses to volcanic eruptions are

discussed in section 4. Finally, a summary is given in section 5.

2. Data and methodology

a. Reconstructed and model data

In this study, eastern China is defined as the area of 25°–41°N, 105°–122°E. This region is chosen to be consistent with the reconstruction data, that is, the 10-yr running mean regionally averaged dry–wet index of Zheng et al. (2006). The dry–wet index was developed from the annual drought/flood grade series of 48 sites over eastern China that were reconstructed originally based on climatic information from Chinese historical documents and instrumental measurements (Zheng et al. 2006). The dry–wet index is a normalized time series of annual resolution in the period 501–2000, and can be used to infer long-term changes in annual precipitation (Zheng et al. 2006). During the overlapping coverage periods, the dry–wet index data were compared with the following independent data: 1) instrumental observations of precipitation in Beijing (1870–1950), Nanjing (1905–36), and Shanghai (1873–1950), and reconstructed precipitation (1736–1950) in the middle and lower reaches of the Yellow River derived from snow and rainfall records in the archives of the Qing Dynasty (Zheng et al. 2005); and 2) reconstructed annual precipitation series at Nanjing, Suzhou, and Hangzhou (Zhang and Wang 1989; Zhang et al. 2005), as well as the precipitation series in the mei-yu season over the lower reach of the Yangtze River (Zhang and Wang 1991). Similar variability is observed in the reconstruction as compared to each of the independent datasets during the period of overlap. This dry–wet index dataset has been widely used in previous studies with the focus on the precipitation changes in China during the last millennium (e.g., Ge et al. 2007; Chen et al. 2010; Graham et al. 2011; Chu et al. 2012; Ren et al. 2012; Chen et al. 2015). Besides the dry–wet index, the MADA data (Cook et al. 2010) are also used for verification of the definition of decadal megadroughts in this study, and for quantification of the characteristics of observed decadal megadroughts.

The simulations are derived from the CESM-LME archive generated by the CESM Paleoclimate Working Group at the National Center for Atmospheric Research, with ~2° resolution for the atmosphere and land components and ~1° resolution in the ocean and sea ice components (Otto-Bliesner et al. 2016). Because this study mainly focuses on the influences from volcanic eruptions, one control experiment (CTRL) and five volcanic eruption sensitivity experiments (VOLC) from the CESM-LME archive extending from 850 to 1850 are used herein. The VOLC experiments are forced by the same volcanic forcing only. The volcanic forcing is based on the transient time series of the volcanic sulfate aerosol reconstructed from ice cores (Gao et al. 2008). The simulated monthly sea level pressure (SLP) and u- and v-component winds from both experiments are used to represent the synoptic climate circulation patterns that directly influence the decadal megadroughts over eastern China, while the SSTs are used to examine the thermal anomalies inducing the circulation patterns.

Through the comparisons with various observations and reconstructions (e.g., coral proxy data, NADA, MADA), previous studies (e.g., Otto-Bliesner et al. 2016; Stevenson et al. 2016, 2017, 2018) have shown that the CESM model is able to reproduce reasonably well ENSO and AMO variability during the last millennium in their power spectra and patterns, the El Niño–like response to large volcanic eruptions, and ENSO- and AMO-associated teleconnections on global droughts. CESM has also been widely used in the investigation of the detailed mechanisms behind the ENSO and AMO responses to large volcanic eruptions (e.g., Stevenson et al. 2016; Sun et al. 2019).

b. Definition of decadal megadrought

There is no objective definition for a "megadrought." Some definitions are based on soil moisture deficits, while some others are based on precipitation deficits (Meehl and Hu 2006). Because the reconstructed data used in this study are precipitation data, we chose a definition of megadrought based on sustained precipitation deficits. Therefore, in this study, to focus on decadal-scale megadroughts, the standardized regional area-averaged precipitation anomalies are first low-pass filtered with a 11-yr running mean, to be consistent with the reconstruction data (Zheng et al. 2006). A megadrought is defined as a period in which precipitation anomalies are, first, less than zero for at least 11 consecutive years and, second, less than one standard deviation for at least one year on the low-pass filtered data. Similar definitions considering both duration and magnitude thresholds were widely used in previous studies (e.g., Ault et al. 2018; Stevenson et al. 2018).

3. Results

a. Reconstructed and simulated decadal megadroughts

Figure 1a shows the time series of the reconstructed dry–wet index and Palmer drought severity index (PDSI) from the MADA data over eastern China with decadal megadroughts marked in gray. During the

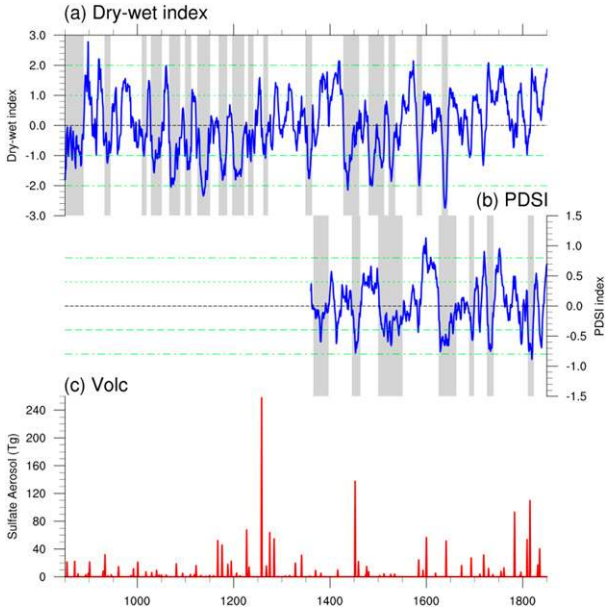

FIG. 1. The time series of the (a) standardized reconstructed dry–wet index, (b) PDSI index, and (c) volcanic sulfate aerosol (red lines; Tg) with decadal megadroughts highlighted in gray. The black solid lines indicate the mean values. The green dashed lines indicate ±1 and ±2 standard deviations.

period 850–1850, there are 18 decadal megadroughts in the reconstructed dry–wet index. During the overlap period 1350–1850, there are four megadroughts based on both dry–wet index and PDSI. The identified decadal megadroughts from the dry–wet index are consistent with Zheng et al. (2006), including several severe droughts that might have influenced the Chinese history significantly (e.g., the Ming Dynasty drought around 1640). This indicates that the definition of decadal megadroughts used in this study is robust.

Using the definition of megadrought established in section 2b, in the period of 850–1850 the single CTRL experiment has 18 megadroughts based on precipitation and 16 megadroughts based on PDSI. These megadroughts are caused by internal climate variability, because there is no external forcing imposed. With the volcanic forcing, the 5-member VOLC experiments have 14 ± 2.74 megadroughts based on precipitation and 12.4 ± 1.14 megadroughts based on PDSI (Table 1). This seems to suggest that the frequency of megadroughts is reduced in the VOLC experiments than in CTRL. Given the small sample size of the experiments and strong internal climate variability intrinsic to the climate system, however, the difference of the frequency of the megadroughts need to be tested statistically. Here, this is tested using a Monte Carlo approach with a 2000-member simulation of red noise. Figures 2a and 2b show one example of red noise, in both the time series

TABLE 1. The frequencies of the decadal megadroughts from the reconstructions, the CTRL experiment, and the five VOLC experiments.

	Frequency	Frequency based on PDSI
Reconstruction	18	9 (1360–1850)
CTRL	18	14
VOLC_1	12	14
VOLC_2	17	13
VOLC_3	17	11
VOLC_4	12	12
VOLC_5	12	12
Average of VOLC (standard deviation)	14 (2.74)	12.4 (1.14)

and power spectrum. Following the method from previous studies (e.g., Ault et al. 2014), the red noise here is reconstructed from an autoregression process of the same autocorrelation coefficient as the reconstructed PDSI in its original annual resolution ($r_1 = 0.27$). The probability distribution produced by the 2000 red noise shows a peak at 16 megadroughts during each period of 1000 years (Fig. 2c). Moreover, the PDF distribution extends from about 9 to 22 megadroughts, with the 95% and 90% confidence intervals at (11.43, 19.55) and (12.07, 18.89), respectively. Therefore, the drought frequencies in the single CTRL experiment, 2 (of 5) VOLC experiments based on precipitation, and 2 (of 5) VOLC experiments based on PDSI, are not significantly different from the red noise. However, the frequencies in the other 3 (of 5) VOLC experiments based on precipitation (12 megadroughts), and the other 3 (of 5) VOLC experiments based on PDSI (11 or 12 megadroughts; see Fig. S2 in the online supplemental material), as well as the frequency in the ensemble mean precipitation of all 5 VOLC experiments (12 megadroughts; see Fig. S1a), are all below the 90% confidence interval based on red noise Monte Carlo simulations. This suggests that, in CESM, volcanic forcing alone may reduce the frequency of megadrought occurrences to be significantly lower than the CTRL experiment, at the 90% significance level. The Monte Carlo method has been widely used in previous studies (e.g., Delworth and Zeng 2014). The particular Monte Carlo method based on red noise time series used in the current study is adapted from Ault et al. (2014), which used a similar method to investigate the megadrought occurrences over the U.S. Southwest during the last millennium. Considering the underlying continuum of hydroclimate and autocorrelations of the drought indices due to the memory of surface moisture (Ault et al. 2014), the Monte Carlo method using red noise time series provides a more reasonable test of the

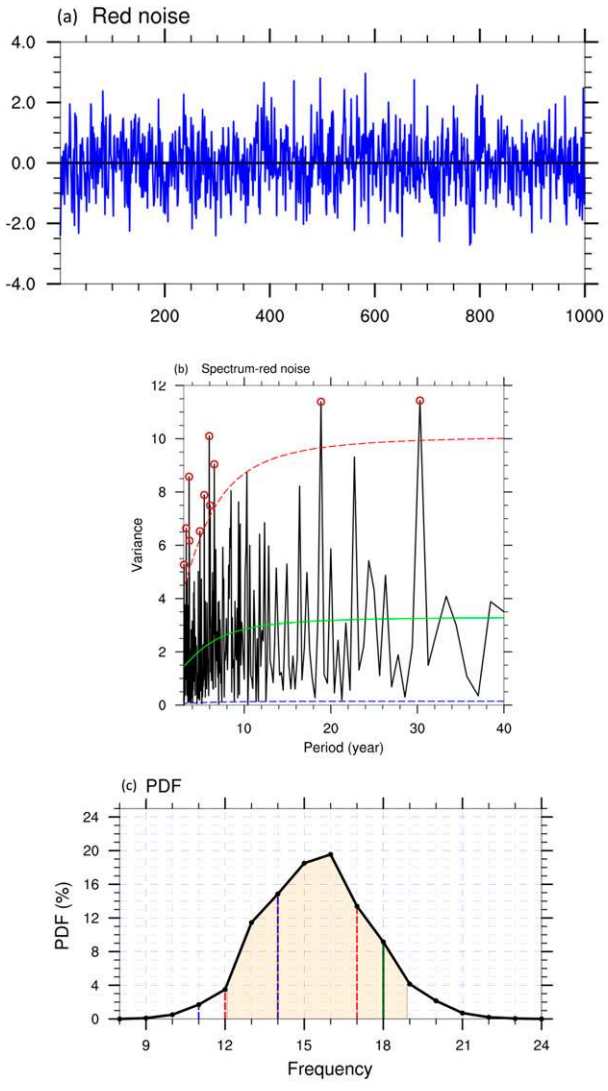

FIG. 2. (a) The samples of red noise time series used in the 2000-member Monte Carlo simulation, (b) spectra of the red noise time series, and (c) the corresponding probability distributions structured from red noise time series (black) with the 90% confidence intervals marked as yellow shaded area. In (c), the megadrought frequencies based on precipitation and PDSI in CTRL are shown as a vertical green solid line (18) and vertical orange solid line (14), and the megadrought frequencies based on precipitation and PDSI in VOLC are shown as vertical red dashed lines (12–17) and vertical blue dashed lines (11–14).

characteristics of megadroughts in previous studies (e.g., Coats et al. 2013; Stevenson et al. 2015; Ault et al. 2018).[1]

[1] We also performed the test with a white noise annual time series, with similar results. This occurs because the 11-yr running mean leads to a significant reddening of a time series, even a white noise (autocorrelation 0.91 on a white noise $r_1 = 0$, compared with 0.95 on our red noise of $r_1 = 0.27$). Therefore, the test results are not very sensitive to the annual autocorrelation of the time series.

Detailed analyses on how volcanic eruptions influence the decadal megadrought frequency and evolution will be presented in section 3b.

b. *Mechanism behind the decadal megadroughts*

The composites of SSTA associated with the decadal megadroughts in the CTRL experiment (Fig. 3a) show a tripolar pattern with negative SSTA over the northwestern Pacific surrounded by positive SSTA from the western tropical Pacific to high latitudes, resembling a positive Pacific decadal oscillation (PDO) pattern with some differences (e.g., an increase in the tropical zonal SST gradient). This pattern is also found in a previous study to be relevant to multidecadal megadroughts over eastern China (Ning et al. 2019), indicating this SSTA pattern could be a dominant driver of hydroclimate over eastern China (Cook et al. 2016; Stevenson et al. 2018). This is further confirmed by the composites of SSTA of 3-, 2-, and 1-yr periods leading the megadroughts (Figs. S3a–c), which show that this SSTA pattern emerges before the occurrences of megadroughts.

The composite of SLP anomalies relevant to the SSTA patterns show negative anomalies over the western tropical Pacific and northeastern Asia and positive anomalies over eastern China (Fig. 3b). Consistent with the SSTA pattern, this SLP anomaly pattern also emerges before the occurrences of megadroughts (Figs. S3d–f). The 700-hPa wind anomalies corresponding to the SLP anomalies show an anomalous cyclonic circulation over the northwestern Pacific at about 19°N, with northerly wind anomalies over southeastern China during the summer monsoon season (May–September) (Fig. 3c). Following previous studies on the volcanic influence on precipitation over eastern China (e.g., Anchukaitis et al. 2010; Man et al. 2014), we will here focus the analysis of the Asian summer monsoon season, since eastern China is a typical monsoon region. This indicates that a weakening of the western North Pacific subtropical high (WPSH) and also a failure of the EASM drives megadroughts in eastern China, as found in previous studies (e.g., Cook et al. 2010).

Previous studies (e.g., Coats et al. 2015; Stevenson et al. 2015) have suggested that the triggering of megadroughts can result from internal variability of the climate system, in addition to a response to external forcings. This conclusion is confirmed by the EOF analyses on SSTA from the CTRL experiment with the second EOF pattern resembling the SSTA patterns relevant to the decadal megadroughts in Fig. 3a, with strong loadings over the northwestern Pacific (0°–30°N, 105°–130°E) and western tropical Pacific (10°S–10°N, 140°E–170°W), as marked by rectangles in Fig. S4. The occurrence of this pattern in the CTRL experiment

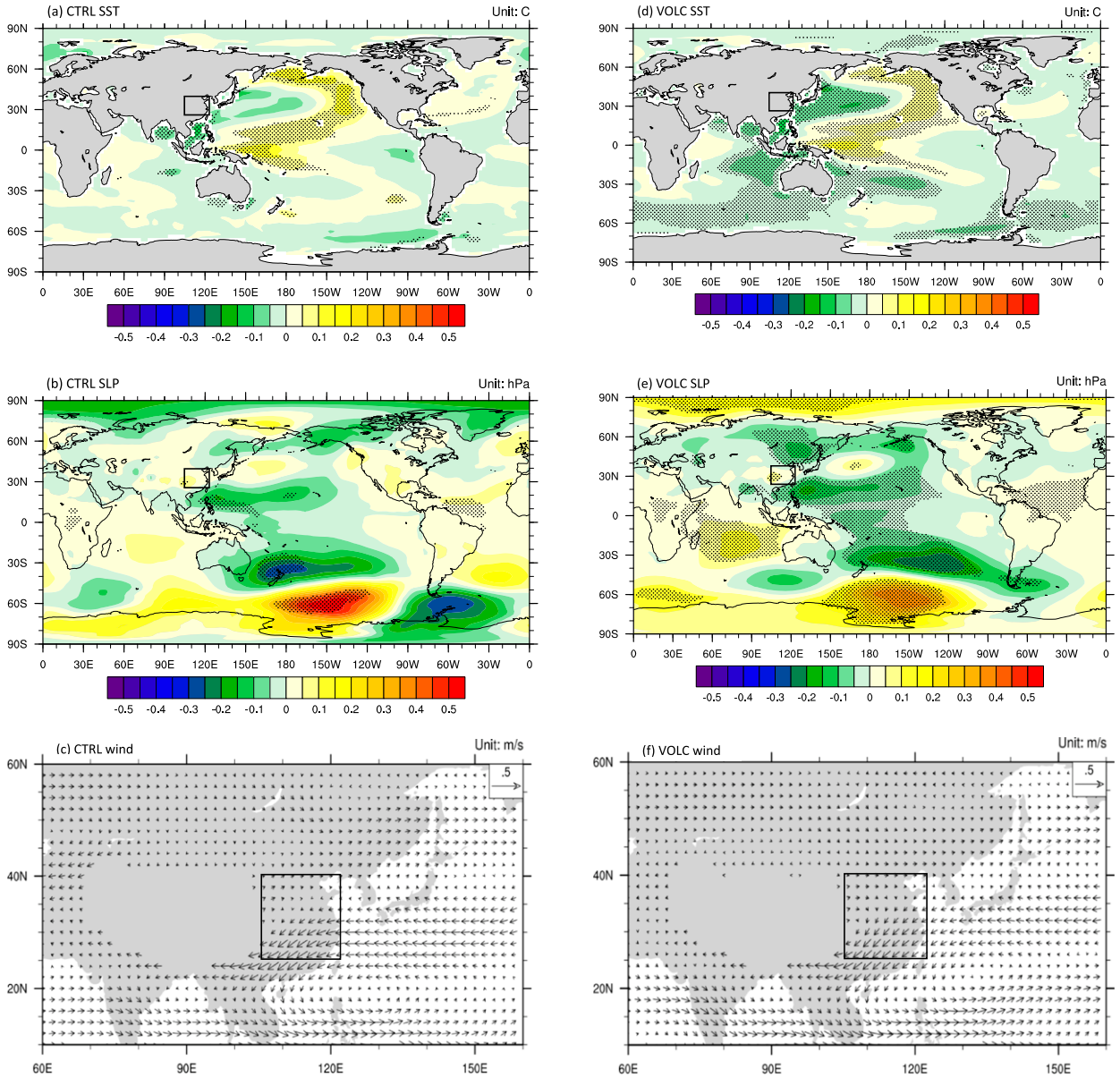

FIG. 3. Composites of simulated ensemble-averaged (a),(d) SSTA (°C), (b),(e) SLP anomalies (hPa), and (c),(f) wind field anomalies at 700 hPa ($m\,s^{-1}$) of the Asian summer monsoon season associated with the megadroughts from the (left) CTRL and (right) VOLC experiments. The rectangle in each panel shows the study region. Stippling indicates differences significant at the 95% level based on Student's *t* test.

indicates that the SSTA pattern relevant to the megadroughts over eastern China can result from internal variability of the climate system. Similar patterns can be found in the EOF analyses of the SSTA from each of the five VOLC experiments, with the variances explained by this EOF pattern around 11% in all the VOLC experiments, close to the percentage (11.6%) in the CTRL experiment (Table S1).

These EOF patterns are significantly correlated with the time series of precipitation anomalies over eastern China after 11-yr running averaging in both the CTRL experiment and VOLC_1 experiment ($p < 0.01$) (Figs. 4a,b), indicating that the decadal megadroughts are relevant to the SSTA patterns with positive EOF principal components (PCs). The results are similar in all VOLC experiments (Table S1). When compositing all the decadal megadroughts together, the PCs show significant positive values during the megadrought periods in both the CTRL experiment and VOLC_1 experiment (Figs. 4c,d). Moreover, when comparing the

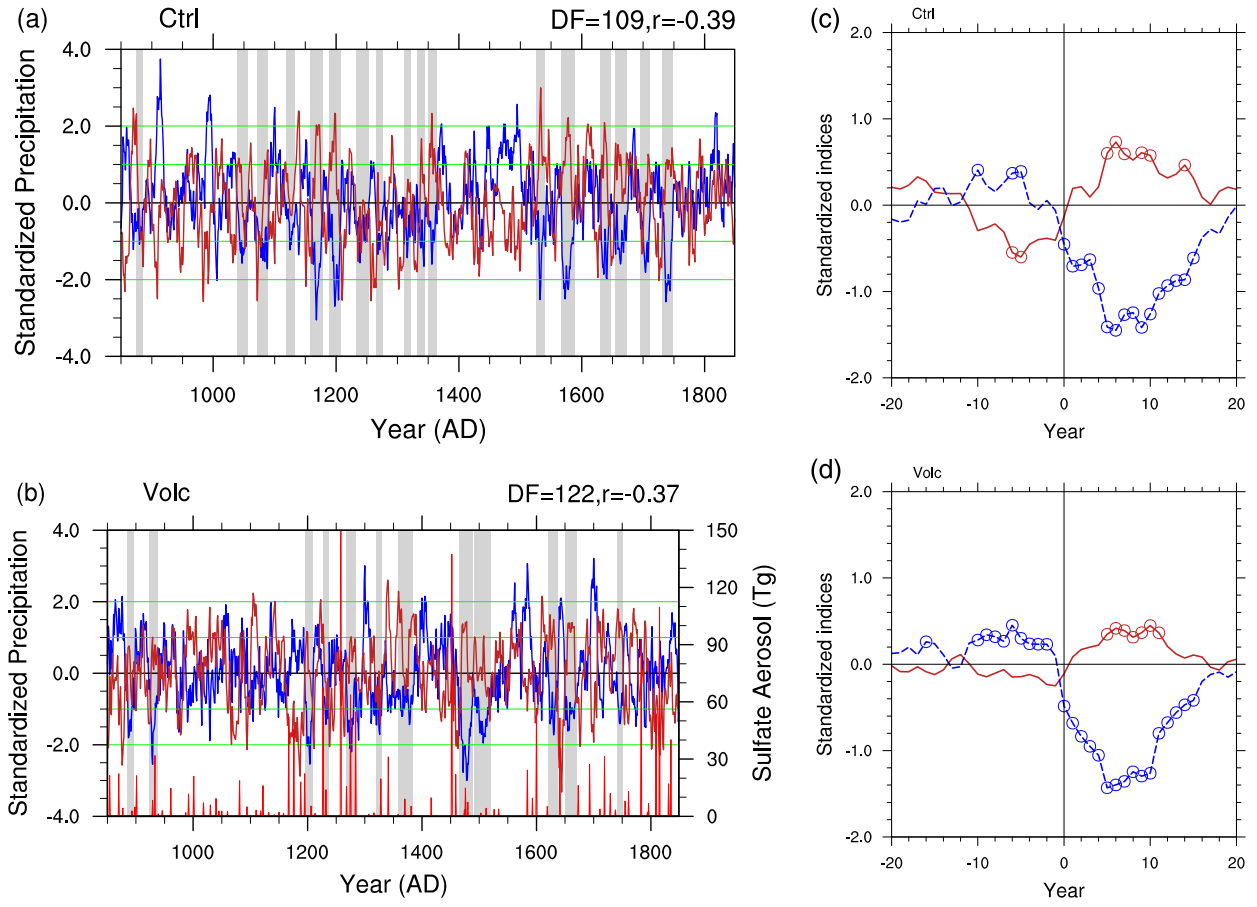

FIG. 4. (a),(b) The time series of the simulated standardized precipitation (blue lines), PCs from EOF analyses (brown lines), and volcanic sulfate aerosol (red lines; Tg) with decadal megadroughts highlighted in gray, and (c),(d) the composites of standardized precipitation (blue lines) and EOF PCs (brown lines) during the megadrought events, from the (top) CTRL and (bottom) VOLC_1 experiments. In (a) and (b), the black solid lines indicate the mean values. The green dashed lines indicate the ±1 and ±2 standard deviations. In (c) and (d), the open circles indicate the anomalies are significant at the 95% level from 0 based on Student's *t* test.

timing between reconstructed megadroughts (Fig. 1) and simulated megadroughts (Figs. 4a,b), there are obvious disagreements between the reconstruction and each simulation, and between the CTRL experiment and the VOLC experiments. This disagreement is also consistent with a dominant internal variability, instead of external forcings, as the triggering mechanism of the megadroughts in the climate system (Coats et al. 2013), unless the volcanic forcing is unrealistically implemented in CESM, or that CESM unrealistically responds to this forcing.

c. *Influences from strong volcanic eruptions*

We further examine how volcanic eruptions modulate the frequency and evolution of the decadal megadroughts. In this section, the 10 strongest volcanic eruptions during the period 850–1850 are first selected, namely, 1167, 1227, 1258, 1275, 1284, 1452, 1600, 1783, 1809, and 1815 (Gao et al. 2008). Then, the influences on regional precipitation anomalies from the volcanic eruptions on interannual scale and decadal scale are investigated through composite analyses.

A composite of the precipitation anomalies after all strong volcanic eruptions from the VOLC experiments (Fig. 5a) show significant decreases over eastern China at the year of eruptions and also the first year after eruptions, which has been discussed in many previous studies (e.g., Man et al. 2014). This is also consistent with the dry conditions over eastern China after strong volcanic eruptions found in previous studies based on both proxy data and model simulations, with smaller responses in the proxy data (Anchukaitis et al. 2010). From the second year after the eruptions, negative precipitation anomalies shift to positive anomalies with significant anomalies at the third year. Then, the precipitation anomalies shift to significantly negative at the

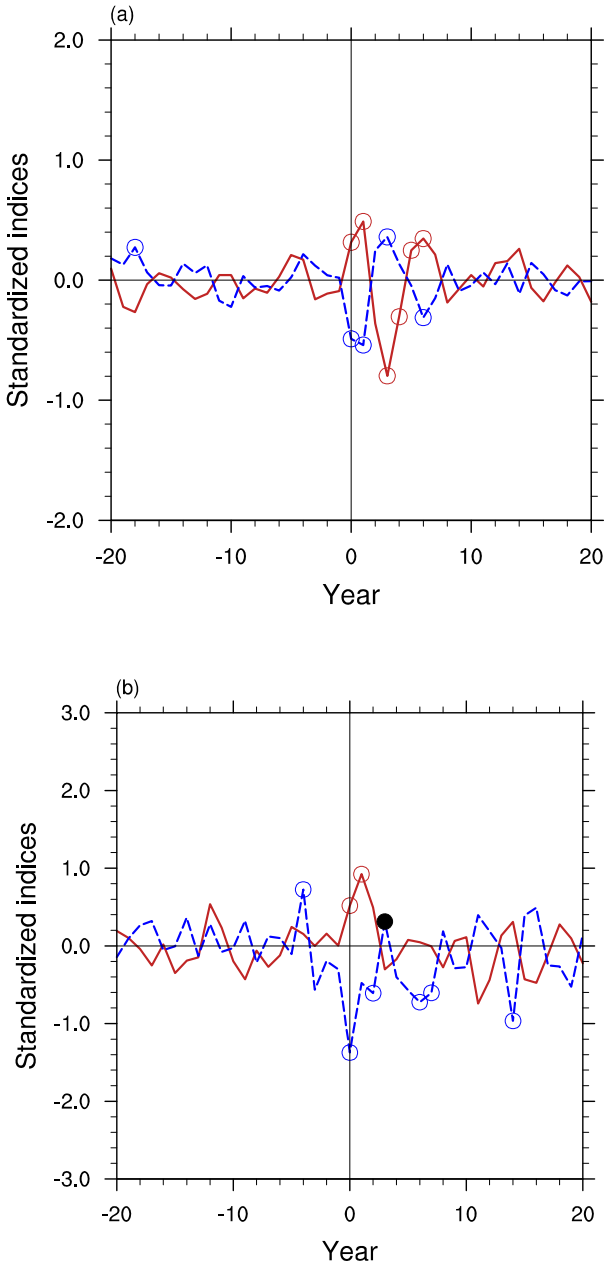

FIG. 5. The changes of standardized precipitation (blue lines) and PCs from EOF analyses (brown lines) after (a) all volcanic eruptions and (b) volcanic eruptions coincided that with decadal megadroughts. The open circles indicate the anomalies are significant at the 95% level from 0 based on Student's *t* test. The solid circles in (b) indicate the precipitation anomalies are significantly different from precipitation anomalies during the decadal megadroughts at the 95% level based on Student's *t* test.

6th year, which ends at the 10th year after volcanic eruptions.

This oscillation within the precipitation anomalies, which we refer to hereinafter as a damping process, is consistent with the evolution of PCs from EOF analyses, which show significant positive anomalies during the first and second year after volcanic eruptions and then significant negative anomalies during the third and fourth year. During the 5th and 6th year, the PCs shift to significant positive anomalies again, and this damping process also ends around the 10th year after volcanic eruptions.

To examine this evolution of SSTA and precipitation anomalies in detail, the SSTA, SLP, and wind anomalies at the year of eruptions and each year after eruptions are shown in Figs. S5 and S6. From the evolution of the SSTA (Fig. S5), we can see that there are negative SSTA globally with larger anomalies over the northwestern Pacific and eastern tropical Pacific during the years of eruptions (Fig. S5b). During the first year after the eruption, the magnitude of the negative SSTAs over the northwestern Pacific continues to grow, while a strong El Niño appears over the eastern tropical Pacific (Fig. S5c). The SSTA magnitude of this pattern decreases during the second year after an eruption (Fig. S5d) and then shifts to a strong La Niña state persisting from the third year to the fifth year (Figs. S5e–g), similar to multiyear La Niña events found in previous studies (DiNezio and Deser 2014; Okumura et al. 2017). This ENSO phase transition is influenced by the volcanic eruptions, as found in previous studies based on proxy reconstructions (e.g., Adams et al. 2003; McGregor et al. 2010) and model simulations (e.g., McGregor and Timmermann 2011; Maher et al. 2015; Wang et al. 2018; Sun et al. 2019), which all show a significant increase of the probability of La Niña events following El Niño events after strong volcanic eruptions. The mechanism behind this transition from an El Niño to La Niña state in response to strong volcanic eruptions has been investigated in detail in our previous study (Sun et al. 2019). After the fifth year, there is also a similar shift from El Niño to La Niña with much weaker SSTA (Figs. S5h–l).

The corresponding patterns of SLP anomalies and 700-hPa wind anomalies (Fig. S6) show a weakening EASM with a negative SLP anomaly over the western subtropical Pacific during an eruption year and the first year after eruption (Figs. S6b,c). Then, the EASM is strengthened with positive SLP anomalies over the western subtropical Pacific (Figs. S6d–f) due to the Kelvin wave–like propagation corresponding to the shift from El Niño to La Niña (Fig. S5), consistent with positive precipitation anomalies during this period. From the fifth year (Figs. S6h–l), another shift from weak EASM to strong EASM appears and results in corresponding changes of the precipitation anomalies.

Now, we discuss the physical mechanisms behind the two damping processes. During the first damping process occurring from year 1 to year 3, there is a strong El

Niño occurring in the second year (Fig. S5d), inducing an anomalous western North Pacific anticyclone (WNPAC) as found in previous studies (Wang et al. 2000), which tends to enhance anomalous southerlies over southern China and decrease anomalous northerlies over northern China (Fig. S6d), weakening the drought event. In the third year, a La Niña develops over the central-eastern equatorial Pacific (Fig. S5e) and the anomalous WNPAC is enhanced through the wind–evaporation–SST feedback, which strengthens the EASM through the anomalous southerlies (Fig. S5e) (Wang et al. 2000). The second damping process happens after the sixth year. In this time, the equatorial Pacific SST anomalies become much weaker than those during the years 1 to 6 and there is also a similar transition from weak El Niño to weak La Niña (Figs. S5i–l), which weakens the drought events after the sixth year.

Within all VOLC experiments, 10 volcanic eruptions coincide with the megadroughts. The evolution of precipitation anomalies during megadrought events is similar to the evolution of ensemble mean precipitation anomalies after all volcanic eruptions but with more negative initial precipitation anomalies, indicating that these features result from a combination of internal variability and external volcanic eruptions. Another difference between volcanic eruptions with and without megadroughts is that the variance of the precipitation anomalies with megadroughts is larger (ranging from −1.4 to 0.4) than for those without megadroughts (ranging from −0.6 to 0.4), which is consistent with the larger magnitudes of the SSTA during the eruptions with megadroughts (not shown).

After removing the direct influences of strong volcanic eruptions (defined as the global-averaged SSTA), the structure of the SSTA patterns induced by the strong volcanic eruptions partially resemble a negative PDO-like pattern on the decadal time scale with contrasting SSTA between the western tropical Pacific and northwestern Pacific (Fig. S7). This SSTA pattern favor above-normal precipitation anomalies as inferred from the relationships in Fig. 2 and Fig. S4. This is also confirmed by the low-pass filtered SSTA difference between the two key SST regions (black line in Fig. 6), that is, the western tropical Pacific and northwestern Pacific, which show negative values during the decade after volcanic eruptions with significant values around the fourth year. This SSTA pattern favors reduced megadrought risks compared with the SSTA composite (Fig. 3) or EOF patterns (Fig. S4) associated with the megadroughts. This also explains why strong volcanic eruptions do not induce decadal megadroughts, as there are fewer megadroughts in the VOLC experiments than in the CTRL experiment (Table 1). If the volcanic eruptions occur during the megadroughts, these features persist despite the volcanic influence because there are already sufficiently severe drought conditions driven by internal variability (Fig. 5).

To compare the simulations with the proxy reconstruction, two strong volcanic eruptions coinciding with megadroughts from the reconstructed PDSI index were selected, namely the 1452 volcanic eruption and 1809 volcanic eruption (Fig. 1), and the corresponding evolutions of the megadroughts are shown in Fig. 7. Similar to the model simulations (Fig. 5b), the reconstructed PDSI index also shows enhanced drought conditions immediately after volcanic eruptions, then relief from drought conditions, and then back to drought conditions (Figs. 7a,b). Therefore, the megadrought evolutions after strong volcanic eruptions in the proxy reconstruction are similar to those in the model simulations.

4. Discussion

Monsoon precipitation responses to volcanic eruptions and the underlying mechanism have been studied through comparisons between proxy data and model simulations in previous studies (e.g., Anchukaitis et al. 2010; Man and Zhou 2014; Zhuo et al. 2014). Generally, proxy reconstructions and model simulations tend to agree on the average sign of the monsoon response to large eruptions, but discrepancies exist on the magnitudes of responses and over different regions (Anchukaitis et al. 2010).

One potential reason for these discrepancies is that the hydroclimate system itself has a high degree of internal variability in both space and time, so that the hydroclimate response to volcanic forcing is much more spatially heterogeneous (Rao et al. 2017). These discrepancies may also result from the inability of a GCM to capture all of the important ocean–atmosphere dynamics responsible for the influences of explosive volcanism over monsoonal Asia, such as the transient response to diffuse light conditions, the response of monsoon circulation to short-term radiative cooling due to volcanic aerosols, and the balance of radiative and dynamical influences on the monsoon (Anchukaitis et al. 2010). Another potential source of discrepancies between proxy reconstructions and simulations is that the implementation of the volcanic forcing in the GCMs is unable to fully represent the realistic effects of volcanic eruptions (Man et al. 2014).

On decadal scales, responses of megadroughts to volcanic eruptions in our results are consistent with previous findings of a negative PDO-like pattern after strong volcanic eruptions (Wang et al. 2012). However, decadal variability of the EASM under external forcing is weaker than observed, indicating that internal variability of the PDO may play a dominant role in decadal

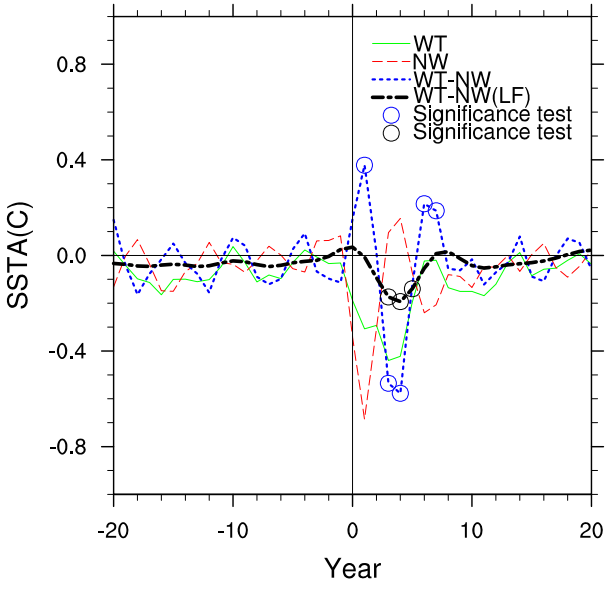

FIG. 6. The changes of SSTA over the western tropical Pacific (green line), northwestern Pacific (red line), difference between western tropical Pacific and northwestern Pacific (blue line), and its low-pass filtered time series (black line) after all volcanic eruptions. The open circles indicate the anomalies are significant at the 95% level from 0 based on Student's *t* test.

monsoon variability (Song et al. 2014). These discrepancies, however, provide important and useful clues for future improvements of the next generation of GCMs (Anchukaitis et al. 2010).

5. Conclusions

The CTRL and five VOLC experiments from the CESM-LME archive were used to examine the influences and mechanisms of volcanic eruptions on decadal megadroughts over eastern China. The direct mechanism for decadal megadroughts is the weakening of the EASM, which results from a meridional tripolar SLP pattern over eastern Asia and a meridional tripolar SSTA pattern over the western Pacific. The SLP pattern includes negative SLP anomalies over northeastern and southeastern Asia, and positive anomalies over eastern China. The SSTA pattern includes negative SSTA over the northwestern Pacific stretching to the northern Indian Ocean, surrounded by a horseshoe pattern of positive SSTA. This SSTA pattern is an internal mode of variability on decadal time scales that explains approximately 11% of the variance in EOF analyses of the model simulations.

On the interannual scale, the SSTAs show an El Niño state on the first year after the eruption, shifting to a La Niña state on the third year after eruption, with a second oscillation of a weaker amplitude within the following

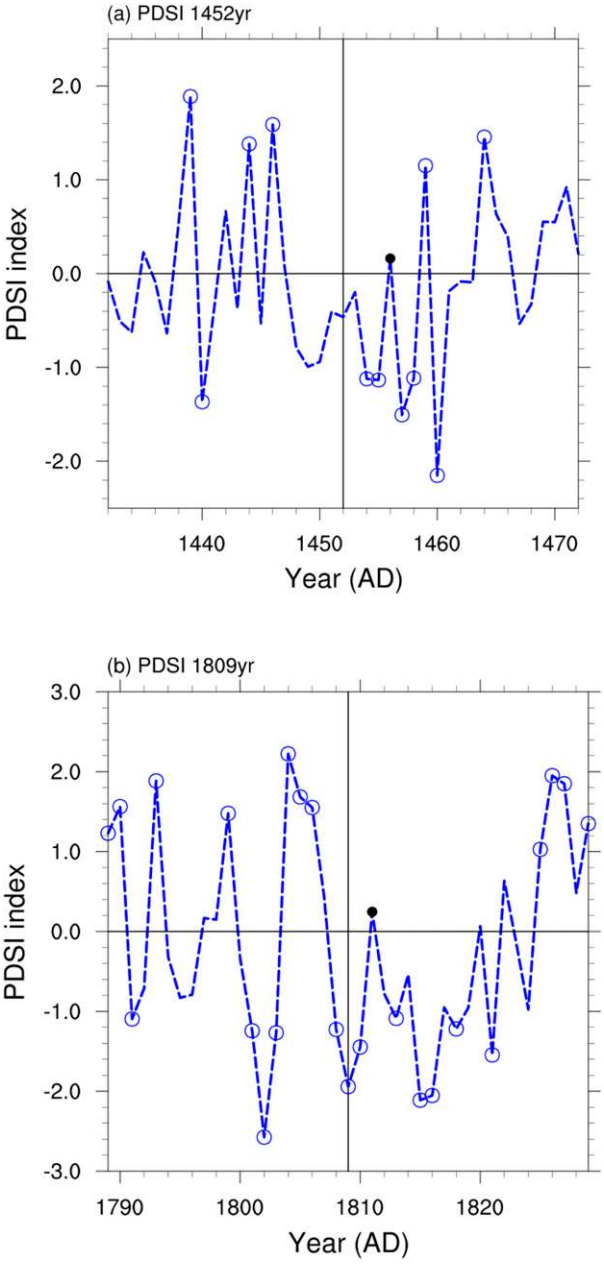

FIG. 7. The evolutions of PDSI index (blue lines) after (a) the 1452 volcanic eruption and (b) the 1809 volcanic eruption that coincided with decadal megadroughts. The open circles indicate the anomalies are significant at the 95% level from 0 based on Student's *t* test. The solid circles in (b) indicate the precipitation anomalies are significantly different from precipitation anomalies during the decadal megadroughts at the 95% level based on Student's *t* test.

decade. The corresponding precipitation anomalies show negative anomalies on the year of eruptions and the following year, but positive anomalies on the third year after the eruptions. When coinciding with megadroughts, the volcanic eruptions first exacerbate the megadroughts, but

then relieve the megadroughts. Therefore, for these features to persist internal variability driving precipitation decreases must be superposed on the volcanic influences.

This is also confirmed by analyses on the decadal scale, which indicate that the SSTA pattern induced by the volcanic eruptions does not favor the occurrence of megadroughts, as the eruptions alter the contrast between SSTA in the western tropical and northwestern Pacific. This helps to explain why the decadal megadrought frequencies seems to be reduced in three of five (based on precipitation) and three of five (based on PDSI) VOLC experiments, at the 90% confidence level based on the red noise Monte Carlo simulations, while the frequencies in the reconstruction and the CTRL experiment are both within the 95% confidence intervals.

This study finds that volcanic eruptions have strong impacts on the evolutions of decadal megadroughts through the modulation of SST and circulation patterns. Our work has important implications for the interpretation of the mechanisms driving decadal megadroughts over eastern China, and also for the direct and indirect influences from volcanic eruptions. Meanwhile, notably, CESM biases could result in some discrepancies when compared with proxy reconstructions. These discrepancies highlight the complexity of regional hydroclimate responses to strong volcanic eruptions (Rao et al. 2017), and also provide important clues for future refinement of GCMs (Anchukaitis et al. 2010). Therefore, current results will not only improve our understanding of regional climate and predictability of future megadrought risks, but also help support strategies for future water resource management, agriculture planning, and societal and economic sustainable developments.

It is interesting to consider our study above in the context of additional experiments. There are 14–19 megadroughts based on precipitation and 13–17 megadroughts based on PDSI in the ensemble of the 13 full forcing experiments during the last millennium (Fig. S8), which are both within the 90% confidence intervals. It is therefore interesting that the megadrought frequencies are consistent in the reconstruction, the CTRL experiment, and the ensemble of the 13 full forcing experiments. To be consistent with the reduction of megadroughts in the VOL experiments, we speculate that the impacts of volcanic eruptions on the reduction of megadrought frequency is canceled out by the collective impacts of all other transient forcings. This speculation, however, remains to be further studied in the future.

Acknowledgments. This research was jointly supported by the National Key Research and Development Program of China (Grant 2016YFA0600401), the National Natural Science Foundation of China (Grants 41971021, 41971108, 41671197, and 41631175), Strategic Priority Research Program of Chinese Academy of Sciences (Grant XDB40000000), and Open Funds of State Key Laboratory of Loess and Quaternary Geology, Institute of Earth Environment, CAS (SKLLQG1820, SKLLQG1930). The CESM-LME data were generated by the CESM Paleoclimate Working Group at NCAR and CESM1(CAM5) Last Millennium Ensemble Community Project, and supercomputing resources are provided by NSF/CISL/Yellowstone. The reconstructed dry-wet index over eastern China was provided by Jingyun Zheng at the Chinese Academy of Sciences. The reconstructed PDSI data (MADA) were kindly provided by Edward R. Cook.

REFERENCES

Adams, J. B., M. E. Mann, and C. M. Ammann, 2003: Proxy evidence for an El Niño-like response to volcanic forcing. *Nature*, **426**, 274–278, https://doi.org/10.1038/nature02101.

Anchukaitis, K. J., B. M. Buckley, E. R. Cook, B. I. Cook, R. D. D'Arrigo, and C. M. Ammann, 2010: Influence of volcanic eruptions on the climate of the Asian monsoon region. *Geophys. Res. Lett.*, **37**, L22703, https://doi.org/10.1029/2010GL044843.

Ault, T. R., J. E. Cole, J. T. Overpeck, G. T. Pederson, and D. M. Meko, 2014: Assessing the risk of persistent drought using climate model simulations and paleoclimate data. *J. Climate*, **27**, 7529–7549, https://doi.org/10.1175/JCLI-D-12-00282.1.

——, J. S. Mankin, B. I. Cook, and J. E. Smerdon, 2016: Relative impacts of mitigation, temperature, and precipitation on 21st-century megadrought risk in the American Southwest. *Sci. Adv.*, **2**, e1600873, https://doi.org/10.1126/sciadv.1600873.

——, S. S. George, J. E. Semerdon, S. Coats, J. S. Mankin, C. M. Carrillo, B. I. Cook, and S. Stevenson, 2018: A robust null hypothesis for the potential causes of megadrought in western North America. *J. Climate*, **31**, 3–24, https://doi.org/10.1175/JCLI-D-17-0154.1.

Chen, F., and Coauthors, 2010: Moisture changes over the last millennium in arid central Asia: A review, synthesis and comparison with monsoon region. *Quat. Sci. Rev.*, **29**, 1055–1068, https://doi.org/10.1016/j.quascirev.2010.01.005.

Chen, J., F. Chen, S. Feng, W. Huang, J. Liu, and A. Zhou, 2015: Hydroclimatic changes in China and surroundings during the Medieval Climate Anomaly and Little Ice Age: Spatial patterns and possible mechanisms. *Quat. Sci. Rev.*, **107**, 98–111, https://doi.org/10.1016/j.quascirev.2014.10.012.

Chu, P., H.-C. Li, C. Fan, and Y.-H. Chen, 2012: Speleothem evidence for temporal-spatial variation in the East Asian summer monsoon since the medieval warm period. *J. Quat. Sci.*, **27**, 901–910, https://doi.org/10.1002/jqs.2579.

Coats, S., J. E. Smerdon, R. Seager, B. I. Cook, and J. F. González-Rouco, 2013: Megadroughts in southwestern North America in ECHO-G millennial simulations and their comparison to proxy drought reconstruction. *J. Climate*, **26**, 7635–7649, https://doi.org/10.1175/JCLI-D-12-00603.1.

——, ——, B. I. Cook, and R. Seager, 2015: Are simulated megadroughts in the North American Southwest forced? *J. Climate*, **28**, 124–142, https://doi.org/10.1175/JCLI-D-14-00071.1.

Cook, B. I., T. R. Ault, and J. E. Smerdon, 2015: Unprecedented 21st century drought risk in the American Southwest and Central Plains. *Sci. Adv.*, **1**, e1400082, https://doi.org/10.1126/sciadv.1400082.

——, E. R. Cook, J. E. Smerdon, R. Seager, A. P. Williams, S. Coats, D. W. Stahle, and J. V. Diaz, 2016: North American megadroughts in the Common Era: Reconstructions and simulations. *Wiley Interdiscip. Rev.: Climate Change*, **7**, 411–432, https://doi.org/10.1002/wcc.394.

Cook, E. R., C. A. Woodhouse, C. M. Eakin, D. M. Meko, and D. W. Stahle, 2004: Long-term aridity changes in western United States. *Science*, **306**, 1015–1018, https://doi.org/10.1126/science.1102586.

——, K. J. Anchukaitis, B. M. Buckley, R. D. D'Arrigo, G. C. Jacoby, and W. E. Wright, 2010: Asian monsoon failure and megadrought during the last millennium. *Science*, **328**, 486–489, https://doi.org/10.1126/science.1185188.

——, and Coauthors, 2015: Old world megadroughts and pluvials during the Common Era. *Sci. Adv.*, **1**, e1500561, https://doi.org/10.1126/sciadv.1500561.

Delworth, T. L., and F. Zeng, 2014: Regional rainfall decline in Australia attributed to anthropogenic greenhouse gases and ozone levels. *Nat. Geosci.*, **7**, 583–587, https://doi.org/10.1038/ngeo2201.

DiNezio, P. N., and C. Deser, 2014: Nonlinear controls on the persistence of La Niña. *J. Climate*, **27**, 7335–7355, https://doi.org/10.1175/JCLI-D-14-00033.1.

Gao, C., A. Robock, and C. Ammann, 2008: Volcanic forcing of climate over the past 1500 years: An improved ice core-based index for climate models. *J. Geophys. Res.*, **113**, D23111, https://doi.org/10.1029/2008JD010239.

Ge, Q., S. Wang, X. Wen, C. Shen, and Z. Hao, 2007: Temperature and precipitation changes in China during the Holocene. *Adv. Atmos. Sci.*, **24**, 1024–1036, https://doi.org/10.1007/s00376-007-1024-7.

Graham, N. E., C. M. Ammann, D. Fleitmann, K. M. Cobb, and J. Luterbacher, 2011: Support for global climate reorganization during the "Medieval Climate Anomaly." *Climate Dyn.*, **37**, 1217–1245, https://doi.org/10.1007/s00382-010-0914-z.

Lu, Z., Z. Liu, J. Zhu, and K. M. Cobb, 2018: A review of paleo El Niño–Southern Oscillation. *Atmosphere*, **9**, 130, https://doi.org/10.3390/atmos9040130.

Maher, N., S. McGregor, M. H. England, and A. S. Gupta, 2015: Effects of volcanism on tropical variability. *Geophys. Res. Lett.*, **42**, 6024–6033, https://doi.org/10.1002/2015GL064751.

Man, W., and T. Zhou, 2014: Response of the East Asian summer monsoon to large volcanic eruptions during the last millennium. *Chin. Sci. Bull.*, **59**, 4123–4129, https://doi.org/10.1007/s11434-014-0404-5.

——, ——, and J. H. Jungclaus, 2014: Effects of large volcanic eruptions on global summer climate and East Asian monsoon changes during the last millennium: Analysis of MPI-ESM simulations. *J. Climate*, **27**, 7394–7409, https://doi.org/10.1175/JCLI-D-13-00739.1.

Mann, M. E., M. A. Cane, S. E. Zebiak, and A. Clement, 2005: Volcanic and solar forcing of the tropical Pacific over the past 1000 years. *J. Climate*, **18**, 447–456, https://doi.org/10.1175/JCLI-3276.1.

McGregor, S., and A. Timmermann, 2011: The effect of explosive tropical volcanism on ENSO. *J. Climate*, **24**, 2178–2191, https://doi.org/10.1175/2010JCLI3990.1.

——, ——, and O. Timm, 2010: A unified proxy for ENSO and PDO variability since 1650. *Climate Past*, **6**, 1–17, https://doi.org/10.5194/cp-6-1-2010.

Meehl, G. A., and A. Hu, 2006: Megadroughts in the Indian monsoon region and southwest North America and a mechanism for associated multidecadal Pacific sea surface temperature anomalies. *J. Climate*, **19**, 1605–1623, https://doi.org/10.1175/JCLI3675.1.

Ning, L., and R. S. Bradley, 2015: Influence of eastern Pacific and central Pacific El Niño events on winter climate extremes over the eastern and central United States. *Int. J. Climatol.*, **35**, 4756–4770, https://doi.org/10.1002/joc.4321.

——, J. Liu, and W. Sun, 2017: Influences of volcano eruptions on Asian summer monsoon over the last 110 years. *Sci. Rep.*, **7**, 42626, https://doi.org/10.1038/srep42626.

——, ——, Z. Wang, and R. S. Bradley, 2018: Different influences on the tropical Pacific SST gradient from natural and anthropogenic forcing. *Int. J. Climatol.*, **38**, 2015–2028, https://doi.org/10.1002/joc.5313.

——, ——, B. Wang, K. Chen, M. Yan, C. Jin, and Q. Wang, 2019: Variability and mechanisms of megadroughts over eastern China during the last millennium: A model study. *Atmosphere*, **10**, 7, https://doi.org/10.3390/atmos10010007.

Okumura, Y. M., P. N. DiNezio, and C. Deser, 2017: Evolving impacts of multiyear La Niña events on atmospheric circulation and U.S. drought. *Geophys. Res. Lett.*, **44**, 11 614–11 623, https://doi.org/10.1002/2017GL075034.

Otterå, O. H., M. Bentsen, H. Drange, and L. Suo, 2010: External forcing as a metronome for Atlantic multidecadal variability. *Nat. Geosci.*, **3**, 688–694, https://doi.org/10.1038/ngeo955.

Otto-Bliesner, B. L., and Coauthors, 2016: Climate variability and change since 850 CE: An ensemble approach with the Community Earth System Model (CESM). *Bull. Amer. Meteor. Soc.*, **97**, 735–754, https://doi.org/10.1175/BAMS-D-14-00233.1.

Palmer, J. G., and Coauthors, 2015: Drought variability in the eastern Australia and New Zealand summer drought atlas (ANZDA, CE 1500–2012) modulated by the interdecadal Pacific oscillation. *Environ. Res. Lett.*, **10**, 124002, https://doi.org/10.1088/1748-9326/10/12/124002.

Peng, Y., C. Shen, H. Cheng, and Y. Xu, 2014: Modeling of severe persistent droughts over eastern China during the last millennium. *Climate Past*, **10**, 1079–1091, https://doi.org/10.5194/cp-10-1079-2014.

Rao, M. P., and Coauthors, 2017: European and Mediterranean hydroclimate responses to tropical volcanic forcing over the last millennium. *Geophys. Res. Lett.*, **44**, 5104–5112, https://doi.org/10.1002/2017GL073057.

Ren, G., Y. Ding, Z. Zhao, J. Zheng, T. Wu, G. Tang, and Y. Xu, 2012: Recent progress in studies of climate change in China. *Adv. Atmos. Sci.*, **29**, 958–977, https://doi.org/10.1007/s00376-012-1200-2.

Shen, C., W.-C. Wang, Z. Hao, and W. Gong, 2007: Exceptional drought events over eastern China during the last five centuries. *Climatic Change*, **85**, 453–471, https://doi.org/10.1007/s10584-007-9283-y.

Song, F., T. Zhou, and Y. Qian, 2014: Responses of East Asian summer monsoon to natural and anthropogenic forcings in the 17 latest CMIP5 models. *Geophys. Res. Lett.*, **41**, 596–603, https://doi.org/10.1002/2013GL058705.

Stahle, D. W., and Coauthors, 2016: The Mexican Drought Atlas: Tree-ring reconstructions of the soil moisture balance during the late pre-Hispanic, colonial, and modern eras. *Quat. Sci. Rev.*, **149**, 34–60, https://doi.org/10.1016/j.quascirev.2016.06.018.

Stevenson, S., A. Timmermann, Y. Chikamoto, S. Langford, and P. DiNezio, 2015: Stochastically generated North American megadroughts. *J. Climate*, **28**, 1865–1880, https://doi.org/10.1175/JCLI-D-13-00689.1.

——, B. Otto-Bliesner, J. Fasullo, and E. Brady, 2016: "El Niño like" hydroclimate responses to last millennium volcanic eruptions. *J. Climate*, **29**, 2907–2921, https://doi.org/10.1175/JCLI-D-15-0239.1.

——, J. T. Fasullo, B. Otto-Bliesner, R. A. Tomas, and C. Gao, 2017: Role of eruption season in reconciling model and proxy responses to tropical volcanism. *Proc. Natl. Acad. Sci. USA*, **114**, 1822–1826, https://doi.org/10.1073/pnas.1612505114.

——, and Coauthors, 2018: Climate variability, volcanic forcing, and last millennium hydroclimate extremes. *J. Climate*, **31**, 4309–4327, https://doi.org/10.1175/JCLI-D-17-0407.1.

Sun, W., J. Liu, B. Wang, D. Chen, F. Liu, Z. Wang, L. Ning, and M. Chen, 2019: A "La Niña-like" state occurring in the second year after large tropical volcanic eruptions during the past 1500 years. *Climate Dyn.*, **52**, 7495–7509, https://doi.org/10.1007/s00382-018-4163-x.

Swingedouw, D., P. Ortega, J. Mignot, E. Guilyardi, V. Masson-Delmotte, P. G. Butler, M. Khodri, and R. Séférian, 2015: Bidecadal North Atlantic Ocean circulation variability controlled by timing of volcanic eruptions. *Nat. Commun.*, **6**, 6545, https://doi.org/10.1038/ncomms7545.

Wang, B., R. Wu, and X. Fu, 2000: Pacific–East Asian teleconnection: How does ENSO affect East Asian climate? *J. Climate*, **13**, 1517–1536, https://doi.org/10.1175/1520-0442(2000)013<1517:PEATHD>2.0.CO;2.

Wang, T., O. H. Otterå, Y. Cao, and H. Wang, 2012: The response of the North Pacific decadal variability to strong tropical volcanic eruptions. *Climate Dyn.*, **39**, 2917–2936, https://doi.org/10.1007/s00382-012-1373-5.

——, D. Guo, Y. Gao, H. Wang, F. Zheng, Y. Zhu, J. Miao, and Y. Hu, 2018: Modulation of ENSO evolution by strong tropical volcanic eruptions. *Climate Dyn.*, **51**, 2433–2453, https://doi.org/10.1007/s00382-017-4021-2.

Yancheva, G., and Coauthors, 2007: Influence of the intertropical convergence zone on the East Asian monsoon. *Nature*, **445**, 74–77, https://doi.org/10.1038/nature05431.

Yang, Q., Z. Ma, X. Fan, Z.-L. Yang, Z. Xu, and P. Wu, 2017a: Decadal modulation of precipitation patterns over eastern China by sea surface temperature anomalies. *J. Climate*, **30**, 7017–7033, https://doi.org/10.1175/JCLI-D-16-0793.1.

——, ——, and B. Xu, 2017b: Modulation of monthly precipitation patterns over east China by the Pacific decadal oscillation. *Climatic Change*, **144**, 405–417, https://doi.org/10.1007/s10584-016-1662-9.

Zhang, D. E., and P. K. Wang, 1989: Reconstruction of the 18th century summer precipitation series of Nanjing, Suzhou, and Hangzhou using the clear and rain records of Qing Dynasty. *Acta Meteor. Sin.*, **3**, 261–278.

——, and ——, 1991: A study on the reconstruction of the 18th century meiyu (plum rains) activity of Lower Changjiang (Yangtze) Region of China. *Sci. China*, **34B**, 1237–1245.

——, Y. W. Liu, Y. Y. Liang, and J. Li, 2005: Reconstruction of annual and seasonal precipitation series of Nanjing, Suzhou and Hangzhou during the 18th century (in Chinese). *Quat. Sci.*, **25**, 121–128.

——, H.-C. Li, T.-L. Ku, and L. Lu, 2010: On linking climate to Chinese dynastic change: Spatial and temporal variations of monsoonal rain. *Chin. Sci. Bull.*, **55**, 77–83, https://doi.org/10.1007/s11434-009-0584-6.

Zhang, L., and T. Zhou, 2015: Drought over East Asia: A review. *J. Climate*, **28**, 3375–3399, https://doi.org/10.1175/JCLI-D-14-00259.1.

Zhang, P., and Coauthors, 2008: A test of climate, sun, and culture relationships from an 1810-year Chinese cave record. *Science*, **322**, 940–942, https://doi.org/10.1126/science.1163965.

Zheng, J. Y., Z. X. Hao, and Q. S. Ge, 2005: Variation of precipitation for the last 300 years over the middle and lower reaches of the Yellow River. *Sci. China*, **48D**, 2182–2193, https://doi.org/10.1360/03yd0392.

——, W.-C. Wang, Q. S. Ge, Z. Man, and P. Zhang, 2006: Precipitation variability and extreme events in eastern China during the past 1500 years. *Terr. Atmos. Oceanic Sci.*, **17**, 579–592, https://doi.org/10.3319/TAO.2006.17.3.579(A).

Zhuo, Z., C. Gao, and Y. Pan, 2014: Proxy evidence for China's monsoon precipitation response to volcanic aerosols over the past seven centuries. *J. Geophys. Res. Atmos.*, **119**, 6638–6652, https://doi.org/10.1002/2013JD021061.